ADVANCED MATERIALS TECHNOLOGIES
www.advmattechnol.de

Polypyrrole Electrodes Show Strain-Specific Enhancement of Photocurrent from Cyanobacteria

Charlotte Roullier, Melania Reggente, Pierrick Gilibert, and Ardemis A. Boghossian**

The discovery of extracellular electron conduits has spurred new applications in microbial electronics. Except for a limited number of exoelectrogens, most microbes are surrounded by insulating membranes that impair extracellular electron transfer. This study focuses on the fabrication of a conductive polypyrrole (PPy) coating for enhancing microbial charge extraction. The polymer deposition is characterized and optimized using a combination of potentiodynamic and potentiostatic measurements as well as scanning electron microscopy (SEM), energy dispersive X-Ray (EDX) analysis, and Raman spectroscopy. The electrodes are used to extract photosynthetic electrons from the cyanobacteria *Synechocystis sp.* PCC6803 (*Synechocystis*) and *Synechococcus Elongatus PCC7942 (Elongatus)*. The PPy electrode shows a sixfold increase in extracted photocurrent for *Synechocystis* under unmediated conditions compared to bare graphite electrodes. This enhancement is attributed to the decreased resistance and increased electroactive surface area of the PPy electrode. By contrast, *Elongatus* shows no substantial difference in photocurrent between the PPy and bare electrodes. Compared to *Synechocystis* cells, the *Elongatus* cells show limited electrode adherence with weaker charge interactions. These findings lay the framework for designing customized polymer electrodes for strain-specific charge extraction.

1. Introduction

Biophotovoltaics (BPVs) rely on biological processes like photosynthesis for solar electricity production. The incorporation of intact microorganisms in these devices enables a living technology that benefits from sustainability, autonomous production, dynamic repair, and adaptive light harvesting. Using sunlight, oxygenic photosynthetic microorganisms separate charge through water-splitting while actively sequestering CO_2 for biomass production. This process has been used to power small electrical devices in low-resource or even off-grid environments.[1,2]

The most common microbes used for living BPVs are photosynthetic cyanobacteria and unicellular eukaryotic algae.[1] Since charge is extracted from light-driven water-splitting, these organisms can produce currents in the absence of exogenous organic substrates.[3,4] The electrons from the water oxidation are transferred through an electron transport chain (the Z-scheme) to synthesize the essential metabolites nicotinamide adenine dinucleotide phosphate (NADPH) and adenosine triphosphate (ATP).[5–7] Under intense light exposure, excess electrons can be exported extracellularly. When these microorganisms or their isolated photosynthetic components are coupled to an anode, the extracted electrons can be transferred to a cathode to drive a current for water recombination.[1,2,5,6] The key to this process is the extracellular electron transfer (EET) that occurs at the microbe-anode interface. The EET can occur indirectly via a redox mediator that is reduced by the cells and re-oxidized at the anode. The EET can also occur directly, though the mechanism for wildtype cyanobacteria is inefficient and poorly understood.[5–11]

The current bottleneck in living BPVs is the low light-to-current conversion efficiency. This low efficiency is attributed to the poor electron transfer across the insulating cell membrane.[12] This transfer can be improved by using natural photoautotrophs as well as bioengineered strains with enhanced EET.[13–18] The bioengineered strains include microbes that express exogenous mediators[15] and electron-shuttling membrane proteins.[14–16] Additionally, the cell membranes of these microbes can be functionalized with conducting nanomaterials that can enhance EET.[13,17,18]

Most studies to date, however, have largely focused on improving electron transfer through electrode engineering. Electrodes are often based on sustainable carbon materials that are abundant, robust, and low-cost. The surfaces of these electrodes can be modified with micron-sized structures to improve cell interactions.[5,6,17,19,20] The surface can also be modified with conducting polymers (CPs), such as polyaniline (PANI), poly(3,4-ethylenedioxythiophene) (PEDOT), polydopamine (PDA), PPy

C. Roullier, M. Reggente, P. Gilibert, A. A. Boghossian
Institute of Chemical Sciences and Engineering (ISIC)
Ecole Polytechnique Fédérale de Lausanne (EPFL)
Station 6, Lausanne 1015, Switzerland
E-mail: melania.reggente@epfl.ch; ardemis.boghossian@epfl.ch

The ORCID identification number(s) for the author(s) of this article can be found under https://doi.org/10.1002/admt.202201839

DOI: 10.1002/admt.202201839

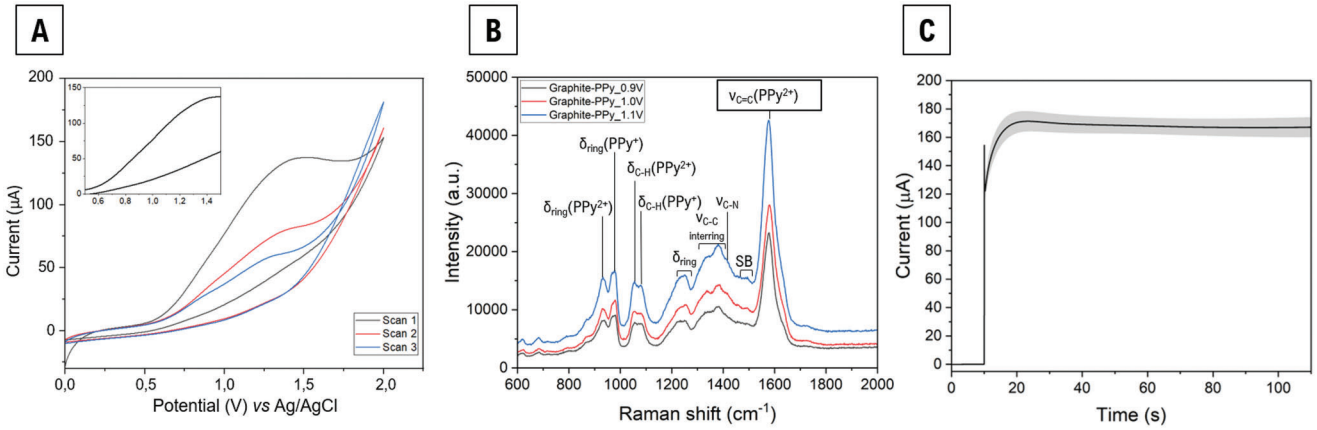

Figure 1. Optimization of dodecyl sulfate-doped PPy polymerization onto graphite electrodes. A) Cyclic voltammetry scans (1 mV s^{-1}) of an aqueous solution of 100 mM pyrrole and 5 mM SDS as the electrolyte, an Ag/AgCl reference electrode, a platinum (Pt) wire as the counter electrode, and a 3-mm diameter graphite rod as the working electrode. Inset: close-up of the first scan in the 0.5–1.5 V (vs Ag/AgCl) range. B) Raman spectra of PPy coatings on graphite rods polymerized at different applied potentials. δ = bending, ν = stretching, SB = skeletal band, PPy^{+} = radical cations (polarons), PPy^{2+} = dications (bipolarons). The signal indicated by the framed label is used to determine the oxidation state of the PPy coating. C) Multistep amperometry measurements monitoring the current onset and evolution during PPy polymerization onto the graphite rod at 1.0 V (vs Ag/AgCl). Measurements were taken following an equilibration time of 10s at 0.0V. The solid line represents the mean value of n = 20 replicates from 4 different batches, and the shaded regions correspond to 1 standard deviation. Individual replicates can be found in Figure S1C, Supporting Information.

and their composites. Such CP-carbon anodes are modular and have consequently been used to boost device efficiencies in different microbial devices.[21–27] PPy in particular was shown to increase the EET of individual cells[23–25] and biofilms[26] of dissimilatory metal-reducing microbes. Compared to metal-reducing microbes, however, applications to cyanobacteria have been much more limited in both scope and success.[6,21,27,28] For example, undoped PPy showed no enhancement in charge extraction from isolated cyanobacteria despite the 4.5-fold improvement that was observed from an unidentified freshwater biofilm.[27,29] Furthermore, the underlying mechanisms for improving charge extraction from cyanobacteria remain largely unexplored, and the design rules for different strains are lacking.

In this work, we design a PPy-based carbon electrode to extract charge from two strains of cyanobacteria, *Synechocystis* and *Elongatus*. The electrode properties were tuned through electrochemical doping of the CP under different polymerization conditions. The engineered electrode selectively increases the extracted photocurrent from the isolated *Synechocystis* strain. The strain-specific enhancement of this electrode was further examined in the framework of cell adhesion and charge interactions. This study thus provides a basis for engineering customized polymer electrodes for pure cultures of cyanobacteria.

2. Results and Discussion

The PPy coating was electropolymerized on graphite using potentiostatic chronoamperometry. The potential used to coat the graphite during this process was chosen based on cyclic voltammetry measurements. These measurements were taken in a 3-electrode system with the graphite substrate as the working electrode and an aqueous solution of pyrrole and sodium dodecyl sulfate (SDS) dopant as the electrolyte.[21] The first scan cycle was used to determine the deposition potential since the initial PPy layer affected the polymerization potential in the following scans. As shown in **Figure 1**A, a current onset in the range of 0.9 to 1.1 V (vs Ag/AgCl) was observed prior to reaching the maximum current peak around 1.4 V (Figure 1A, inset). The initial increase in current is indicative of monomer oxidation, and the maximum corresponds to overoxidation at higher potentials. The PPy was deposited at three different potentials within this range using multistep amperometry. In this protocol, a 10-s equilibration time at 0.0 V (vs Ag/AgCl) was applied before polymerizing for 100 s at 0.9, 1.0, and 1.1 V (vs Ag/AgCl).

Raman spectroscopy was used to confirm the formation of the PPy coating under the tested conditions (Figure 1B).[30,31] The band ascribed to the carbon double-bond stretch ($\nu_{C=C}(PPy^{2+})$) is known to shift to higher wavenumbers with increased polymer oxidation state and conductivity.[28,30,31] In agreement with these findings, we observe a slight shifting of this band at different applied potentials. The electrode polymerized at a potential of 1.0 V showed a slightly higher band wavenumber (1580 cm^{-1}) compared to the ones synthesized at 0.9 V (1579 cm^{-1}) and 1.1 V (1577 cm^{-1}). Additionally, the 1.0 V (vs Ag/AgCl) sample showed a small increase in electroactivity based on cyclic voltammetry measurements in the presence of 1 mM potassium ferricyanide (Figure S1A, Supporting Information). This potential was therefore used to synthesize the PPy electrode for different polymerization times up to 250 s (Figure S2, Supporting Information). In agreement with previous observations, the polymer thickness was found to increase with increasing times (Figure S2C, Supporting Information).[32,33] Although thicker electrodes tend to show higher capacitance, they can increase recombination. Consequently, the most electroactive electrode was obtained after 100 s (Figure S2B, Supporting Information). This polymerization time was thus selected for the PPy electrode in this study. The corresponding amperometry measurements (Figure 1C) show two characteristic regions following the change in potential from 0.0 to 1.0 V (vs Ag/AgCl): an initial peak from the double layer formation followed by a second increase in current that levels out at

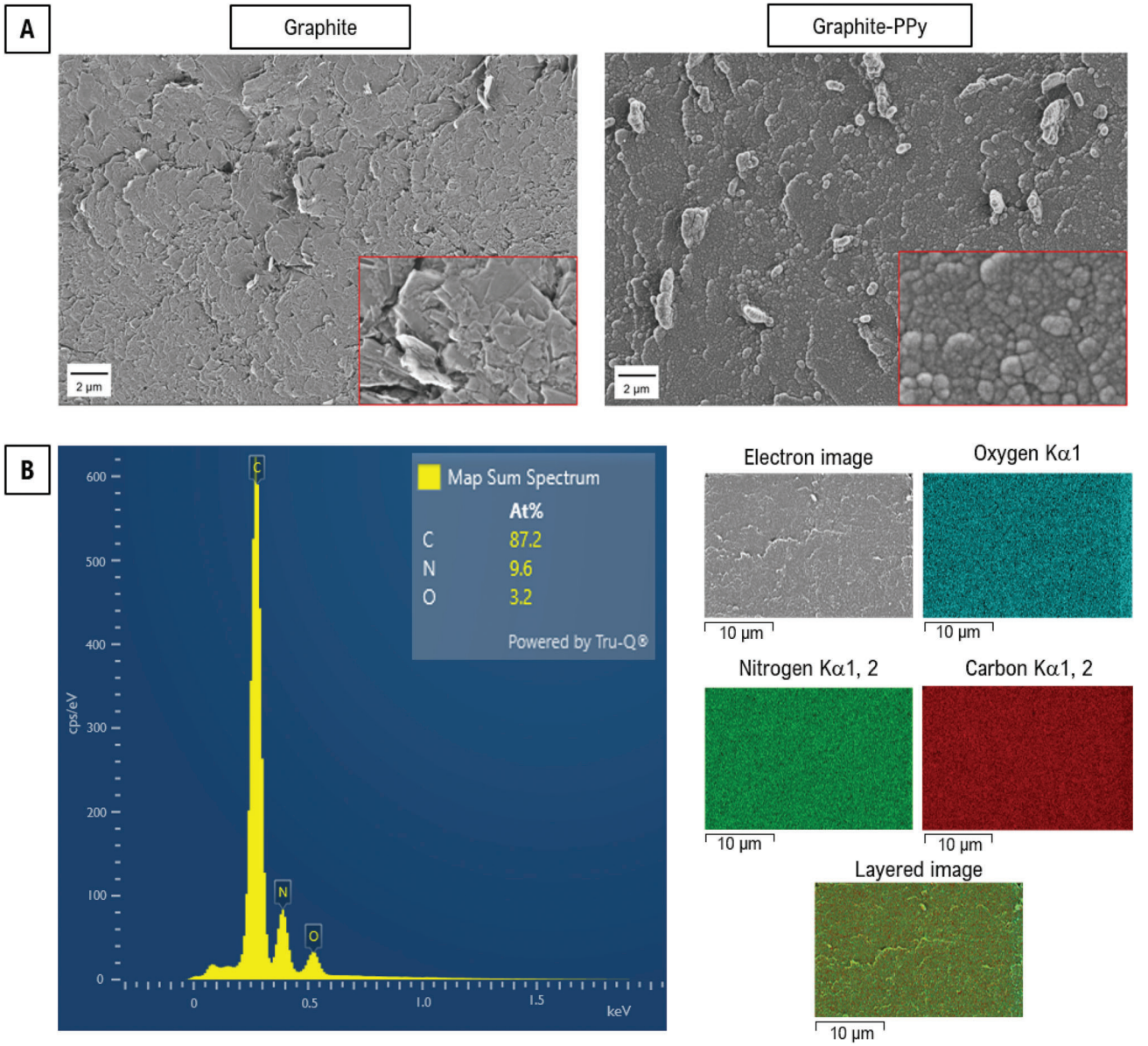

Figure 2. Morphological characterization of PPy-coated graphite electrodes. A) SEM images showing the surface of uncoated graphite (left) and coated (right) graphite with PPy electrosynthesized at 1.0 V (vs Ag/AgCl) for 100 s at 10K magnification (inset: 100K). B) EDX spectrum and mapping of carbon, nitrogen, and oxygen in the PPy coating. The layered image corresponds to the merged electron and elemental maps. The EDX spectrum and mapping of bare graphite can be found in Figure S3, Supporting Information.

longer times. The leveled current corresponds to nucleation and diffusion-controlled growth of the polymer.[21]

The surface morphology of the electrode was characterized using scanning electron microscopy (SEM) (**Figure 2**A). As shown in the figure, the PPy coating shows a homogeneous globular structure. This structure is attributed to the surfactant encapsulation of the monomer prior to polymerization.[30] The formation of the PPy on the graphite substrate was further verified by energy dispersive X-Ray (EDX) (Figure 2B). The EDX measurements showed a uniform distribution of carbon and nitrogen signals from the PPy. Trace amounts of oxygen were also detected on the surface. The oxygen peak likely originates from contamination from exposed air, as it was also detected alongside carbon in the EDX measurements of bare graphite (Figure S3, Supporting Information).

The PPy electrode was subsequently used to extract photocurrent from *Synechocystis*. CA measurements were taken for bare and coated graphite working electrodes in a 3-electrode system under unmediated conditions (**Figure 3**A, inset). The multistep amperometry measurements shown in Figure S4, Supporting Information, were used to determine the optimum potential for the chronoamperometry analysis. Based on these measurements, an applied potential of 0.3 V (vs Ag/AgCl) was used, as this bias showed the highest photoresponse and retention of electrode

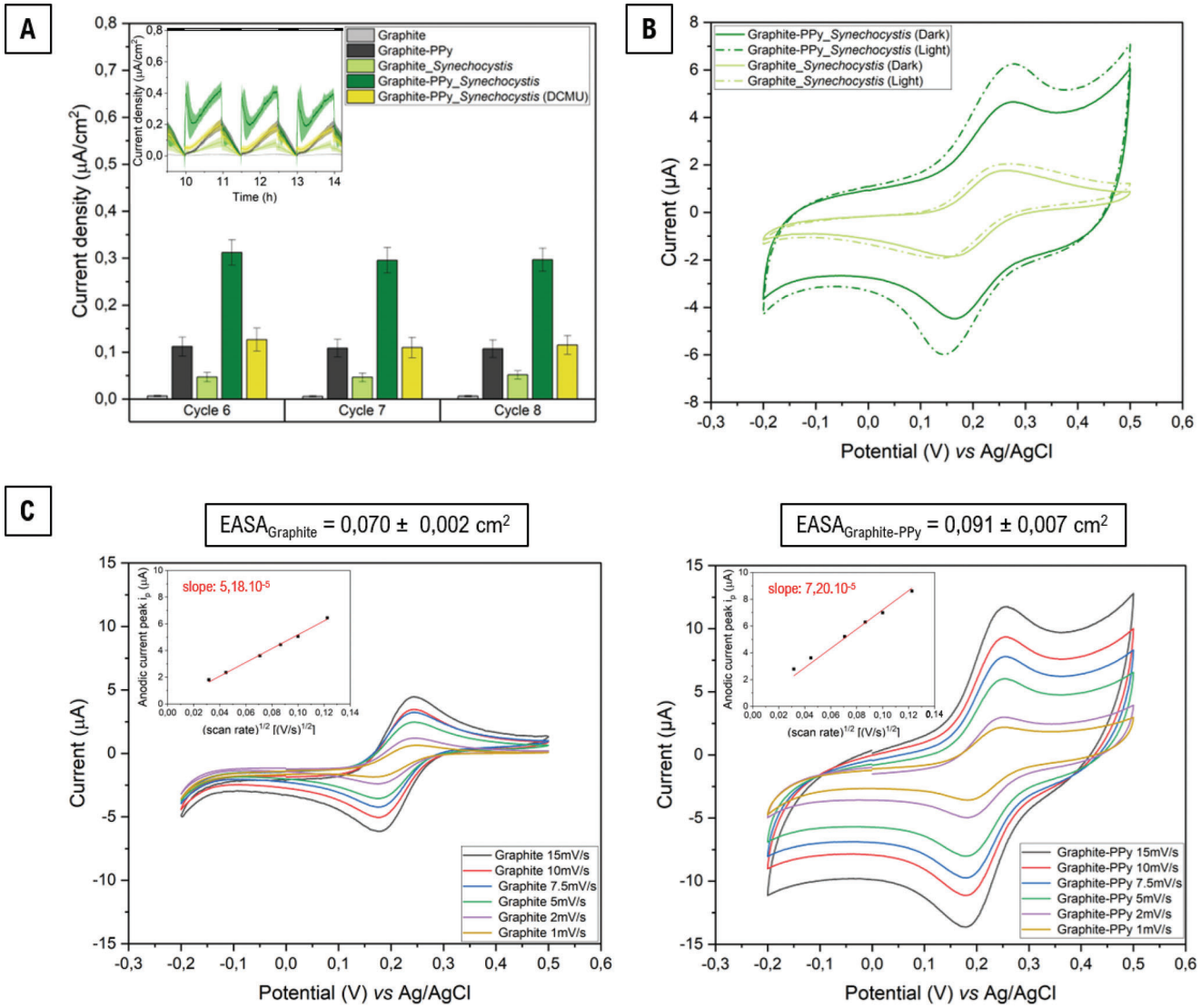

Figure 3. *Synechocystis* photoresponse on PPy-coated graphite electrodes. A) Histogram representing the photocurrent response averaged over the last 40 min of the 6th, 7th, and 8th light cycles for *Synechocystis* on bare graphite (Graphite_*Synechocystis*), *Synechocystis* on PPy-coated graphite (Graphite-PPy_*Synechocystis*), bare graphite in the absence of cells (Graphite), PPy-coated graphite in the absence of cells (Graphite-PPy), and *Synechocystis* on PPy-coated graphite previously pretreated with 50 μM DCMU for 15 min (Graphite-PPy_*Synechocystis* (DCMU)). Error bars represent one standard deviation from the calculated mean for 6 replicates of the graphite-PPy and graphite-PPy_*Synechocystis* samples and 3 replicates for the other samples. Inset: Mean chronoamperometric photocurrent at the corresponding time intervals over t = 10–14 h. Samples were cyclically exposed to dark (black bar) and light (white bar) unmediated conditions. The current density was obtained by dividing current values with the geometrical area of the graphite rod (≈0.71 cm^2) and the normalized current density by additionally dividing with the $chlorophyll_a$ content of the cell pellets (Chl_a (*Synechocystis*) = 5.72 ± 0.03 μg). See Figure S5, Supporting Information, for individual replicates. B) Mediated cyclic voltammograms at a 5 mV s^{-1} scan rate measured in dark and light conditions for *Synechocystis* on bare and PPy-coated graphite. Measurements were taken under mediated conditions in phosphate buffer solution supplemented with 1 mM $K_3Fe(CN)_6$. C) EASA measurements based on cyclic voltammograms recorded in phosphate buffer supplemented with 1 mM $K_3Fe(CN)_6$. Measurements were taken for bare graphite (left) and PPy-coated (right) electrodes. EASA values are given as the mean ± one standard deviation for 3 replicates for bare graphite and 6 replicates (of 4 different batches) for PPy electrodes. Inset: corresponding linear fitting of the anodic current peak intensity versus the square root of the scan rate. Black squares represent the experimental values, and the red line corresponds to the linear fit whose slope is used to calculate the EASA using the Randles–Sevick equation. See Figure S7, Supporting Information, for replicates.

performance. After incubating for 3 h in the dark, the samples were subjected to alternating light-dark cycles. In agreement with Wey et al.,[12] the *Synechocystis* photoresponse on the PPy electrodes shows a characteristic "peak and trough" motif on light exposure. These features are ascribed to the combination of redox-active metabolites and proteins present in the periplasm and extracellular membrane.[12] A steady photoresponse was further achieved after the 4th light cycle, which was maintained until the end of the 15-h measurements (Figure 3A, Figure S5, Supporting Information). As shown in the figure, *Synechocystis* showed a sixfold increase in photocurrent on the PPy electrode compared to *Synechocystis* on the bare graphite electrode. This

enhancement exceeds those reported in previous studies.[24,27] However, we also observed a slight increase in photocurrent from the PPy electrode even in the absence of cells. This finding suggests that the PPy may contribute, at least partially, to the enhancement that was observed in the presence of cells. This hypothesis is consistent with the cyclic voltammetry measurements shown in Figure 3B which show a significant increase in the capacitance of the PPy electrode. To distinguish between the charge extracted from the PPy and from photosynthesis, the *Synechocystis* cells were pre-treated with the photosynthetic inhibitor, 3-(3,4-dichlorophenyl)-1,1-dimethylurea (DCMU).[6] In the presence of DCMU, the *Synechocystis*-incubated PPy electrodes showed a photoresponse that was comparable to PPy electrodes in the absence of *Synechocystis*. Furthermore, the difference between the *Synechocystis*-incubated PPy samples in the absence and presence of DCMU was significantly greater than the photocurrent extracted from *Synechocystis* on bare graphite. These observations show that though the PPy may directly contribute to the photocurrent, the PPy also increases charge extraction from the cells. The decrease observed in the presence of DCMU further shows that this extracted charge comes from photosynthesis.

The underlying mechanism of this enhancement was further studied by cyclic voltammetry. Cyclic voltammograms were taken on freshly made bioanodes in the presence of potassium ferricyanide ($K_3Fe(CN)_6$) (Figure 3B, Figure S6, Supporting Information) under dark and light conditions. As illustrated by the more rectangular shape of the plot, the *Synechocystis*-incubated PPy electrodes showed a substantial increase in capacitance compared to the *Synechocystis*-incubated graphite electrodes, with over a twofold increase in the anodic current peak intensity of the redox species. The PPy samples also show greater sensitivity and shifting of the cathodic current peak to lower potentials on light exposure. This increased sensitivity is consistent with the observed increase in photocurrent. Cyclic voltammetry was also used to compare the electroactive surface area (EASA) of the electrodes. As shown in Figure 3C, the PPy-coated samples showed a 30% increase in the EASA compared to bare graphite samples (Figure S7, Supporting Information). This increase in the EASA of the PPy electrode is consistent with the globular patterned structure observed on the surface of the electrode in Figure 2A. The increased roughness of the surface may therefore contribute to improved contact and more effective charge extraction from the cells. By contrast, the bare graphite showed an EASA that was comparable to the geometrical surface area, indicating a relative lack of roughness.

In addition to the EASA, we compared the sheet resistance and impedance of the electrodes. Four-point probe experiments showed a 17% decrease in the surface sheet resistance of the PPy electrode ($38.21 \pm 0.17 m\Omega\ sq^{-1}$) compared to the bare graphite electrode ($46.37 \pm 0.21 m\Omega\ sq^{-1}$). In addition, the impedance of the electrodes was studied at different frequencies through electrochemical impedance spectroscopy (EIS). The EIS measurements show a substantial difference in the behavior of the two electrodes (Figure S8, Supporting Information). Most notably, the Nyquist plot of the PPy electrode shows solution-controlled behavior with lower charge transfer resistance compared to that of the bare graphite electrode. These observations agree with previously reported spectra from similar materials.[34,35] The results therefore suggest that the decreased material resistance may also contribute to the improved performance of the PPy electrode.

The PPy electrode was then applied to the less common photosynthetic microbe *Elongatus*, which showed a similar photoresponse as *Synechocystis* on the bare graphite electrode (**Figure 4**A). However, in contrast to *Synechocystis*, *Elongatus* showed no substantial increase in photocurrent on the PPy-coated graphite electrode. This difference in photoresponse was studied by comparing the surface charge and adherence of the different strains on the electrode. Zeta potential measurements of the cell suspensions (Figure 4B) showed a less negative potential for the *Elongatus* cells compared to the *Synechocystis* cells. This observation is consistent with the presence of less negatively charged lipopolysaccharides that compose the outer layer of *Elongatus* cells compared to other cyanobacteria.[36,37] This difference may therefore contribute to weaker electrostatic interactions between the cells and the electrode, lowering their adherence to the charged PPy coating. This hypothesis is consistent with previous studies on the charge- and cell-dependent interaction of nanoparticles with different cyanobacteria.[13,38] It is also supported by studies that show improved electrostatic cell interactions with positively charged PPy electrodes.[27,32]

To test this hypothesis, adherence measurements were taken based on chlorophyll$_a$ extraction (Figure 4C and Figure S9, Supporting Information) and crystal violet cell staining (Figure S10, Supporting Information). Whereas the chlorophyll extraction assay measures the relative amount of adhered cells based on their chlorophyll content, the crystal violet assay uses direct cell staining to quantify the relative cell adherence. Both these assays showed a consistent decrease in *Elongatus* adherence and surface coverage on the PPy-based electrode compared to the bare graphite electrodes. These results were corroborated with optical (Figure S11, Supporting Information) and SEM (Figure 4D, Figure S12, Supporting Information) images that similarly show a decrease in cell adhesion. Conversely, *Synechocystis* cells showed similar adherence and surface coverage on both electrodes. These observations confirm that the increased photocurrent from *Synechocystis* is likely due to enhanced charge collection rather than increased cell immobilization.

3. Conclusion

CPs provide a modular basis for optimizing microbe-electrode interactions. The PPy is used in this study to optimize the polymerization of an electrode and to improve charge extraction in a living BPV. This study exploits the formation of the dopant-induced globular surface to increase the EASA of the electrode. The increased EASA, along with increased capacitance and decreased resistance of the electrode, provides a promising avenue for enhancing EET charge extraction. Interestingly, the enhancement in this study was strain-specific, as it was only observed for *Synechocystis*, and not *Elongatus*. This difference is attributed to the more neutral surface charge of the *Elongatus* cells that can lower adherence by weakening the electrostatic interactions with the PPy. The surface chemistry of the microbe is therefore critical in the design of CP-based electrodes. While previous studies explored the effect of strain-specific pili[39–41] and secretions,[42] these studies have only focused on biofilm formation. The decisive effect of surface charge established in this work motivates

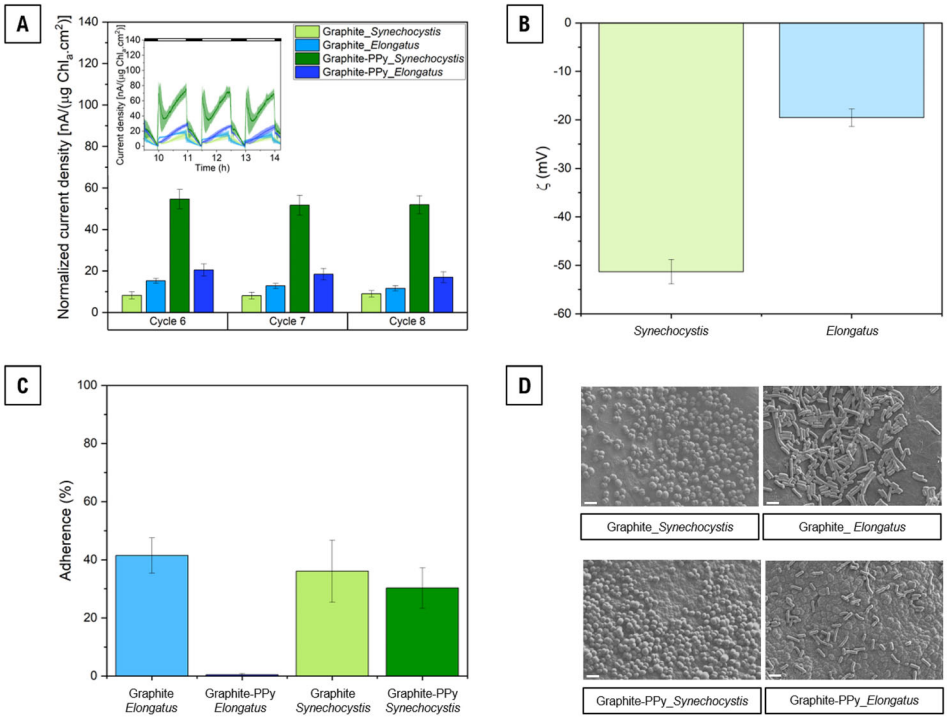

Figure 4. Comparison of *Synechocystis* and *Elongatus* cell-electrode interactions. A) Histogram representing the photocurrent response averaged over the last 40 min of the 6th, 7th, and 8th light cycles for *Synechocystis* on bare graphite (Graphite_*Synechocystis*), *Elongatus* on bare graphite (Graphite_*Elongatus*), *Synechocystis* on PPy-coated graphite (Graphite-PPy_*Synechocystis*), and *Elongatus* on PPy-coated graphite (Graphite-PPy_*Elongatus*). Error bars represent one standard deviation from the calculated mean for 6 replicates of the graphite-PPy_*Synechocystis* samples and 3 replicates for the other samples. Inset: Mean chronoamperometric photocurrent at the corresponding time intervals over t = 10–14 h. Samples were cyclically exposed to dark (black bar) and light (white bar) unmediated conditions. The current density was obtained by dividing current values with the geometrical area of the graphite rod (≈0.71 cm^2) and the normalized current density by additionally dividing with the chlorophyll$_a$ content of the cell pellets (Chl$_a$ (*Elongatus*) = 9,62 ± 0,20 µg – Chl$_a$ (*Synechocystis*) = 5,72 ± 0,03 µg). See Figure S4, Supporting Information, for individual replicates. B) Mean Zeta potential values of *Synechocystis* and *Elongatus* cell suspensions obtained from 3 replicate measurements on 3 different samples for each strain. Error bars correspond to one standard deviation. C) Histogram representing the mean percentage of adherence of *Elongatus* and *Synechocystis* cells on bare graphite and PPy-coated electrodes. The error bars represent the standard deviation from the mean calculated over 3 replicates. See Figures S9 and S10, Supporting Information, for additional information on adherence tests. D) Representative SEM images of *Elongatus* and *Synechocystis* cells on bare graphite and PPy-coated electrodes. See Figure S11, Supporting Information, for optical images and Figure S12, Supporting Information, for replicate images of the biotic electrodes. Scale bar: 4µm.

the need to test the performances of different electrodes on various cell architectures. The diversity and tunability of electropolymerized CPs[32] can be the key to tailoring different electrodes for various electro-microbial applications.

4. Experimental Section

Graphite Electrode Preparation: Graphite rods (3.05 mm diameter, Thermo Scientific) were cut into 2-cm long electrodes. The top surface was polished in a two-step process using P1200 sandpaper (3M Wetordry), followed by P2500 silicon carbide paper (BASi Instruments), until a uniform reflective surface was obtained. For the graphite foil electrodes, graphite foil (0.254 mm thick, thermoscientific) was laser cut in 1-cm diameter disks appended with an additional 5×10 mm strip to allow electrical contact. These substrates were sonicated for 10 min in deionized water first and then in 70 vol% ethanol before air drying.

The exposed electrode surface area was confined for polymerization and for measurements on specific areas of interest. This confinement was done by wrapping the sides of the electrode in the vicinity of the polished surface with parafilm for the 3-mm diameter electrode. For the 1-cm diameter electrode, this confinement was achieved by wrapping the bottom of the strip with parafilm and attaching insulating tape on one side.

Synthesis of Dodecyl Sulfate Doped PPy Layers on Graphite Electrodes: The procedure was adapted from Reggente et al.[23] Briefly, a monomer solution of 100 mM of pyrrole (Sigma Aldrich) was prepared in 5 mM of SDS (Sigma Aldrich) and stirred for ≈4 h. 20 mL of this solution was used as the electrolyte in a 3-electrode system involving either a Pt wire (0.404 mm diameter wire, abcr) as the counter electrode for the rod electrodes, or a (10×15) mm^2 Pt foil (0.1 mm thick, abcr) for the foil electrodes, and a (Ag/AgCl)$^{3M\ KCl}$ reference electrode (Amel Electrochemistry). Electropolymerization was achieved by connecting the electrodes to a Multi-Palmsens4 potentiostat (Palmsens BV) equipped with the Multitrace 4.4 software and by performing multistep amperometry with an equilibration period of 10 s at 0.0 V (vs Ag/AgCl). Equilibration was followed by polymerization at 1.0 V optimally for 100 s in the case of the 3-mm diameter electrodes and 520 s for the 1-cm diameter electrodes. Monomer solution stability was monitored throughout the polymerization by recording the absorbance spectra of 1 mL monomer solution in the (250–900) nm range before and after polymerization. These measurements were compared against a 5 mM SDS solution baseline with a Shimadzu UV-3600 Plus spectrophotometer (Shimadzu Corp.) implemented with the UVProbe 2.50 software. Batches of up to 10 graphite rods could be polymerized in 20 mL solution without affecting the oxidation state of the monomer in solution, while 1–2 graphite foil electrodes could be polymerized in 20 mL monomer solution at a time.

Cyanobacteria Cell Cultures: Precultures were prepared by adding 10 mL 1xBG11 medium[43] to a 100 mL Erlenmeyer flask. The flask was inoculated with healthy cells from a BG11-agar plate. After 16 to 24 h of growth at 30 °C, 180 rpm, and 50 µE, the OD_{750} (i.e., optical density or absorbance at 750 nm) of the cell suspensions reached a value between 2.5 and 5. The cell precultures were diluted in 250 mL Erlenmeyer flasks with fresh 1xBG11 to obtain 20 mL cell cultures with a starting OD_{750} of 0.1 for *Synechocystis* and 0.3 for *Elongatus*. The cell cultures were left to grow for 3 days before harvesting them in their mid-to-late exponential growth stage (OD_{750}≈2.5–3.2).

Bioanode Preparation: Cells grown to their mid-to-late exponential stage were harvested and diluted in 1.5 mL Eppendorf tubes to achieve an OD_{750} = 2 in 1 mL of solution. Samples were pelleted and the supernatant was removed after centrifugation at 5000 rpm for 5 min at room temperature. The pellets were washed three times with 1 mL phosphate buffer saline (PBS) solution (Life Technologies BV). After the fourth and final centrifugation, pellets were gently resuspended in 5 µL PBS and drop-casted onto the polished and polymer-coated 3-mm graphite electrodes. The aliquots were left to settle at room temperature for ≈45 min until a humid, flat pellet was obtained on the electrodes. The cells were secured using a 12.4 MWCO dialysis cellulose membrane (Sigma Aldrich) activated in PBS for 30 min, a Teflon cap (Starlab), and parafilm.

Adherence Test based on Chlorophyll$_a$ Extraction: Bioanodes were prepared as described above up until the addition of the dialysis membrane. Bioanodes were immersed in 1 mL PBS and shaken at 25 °C and 600 rpm for 20 min. The cells remaining at the surface of the electrodes were detached by additional shaking for 20 min at 2000 rpm and by scrapping off the superficial layer of the rod with a metal spatula. Control experiments involving the recovery of the whole pellet in one 1 mL sample were done using the latter shaking conditions. Chlorophyll$_a$ extraction on all samples was performed by pelleting and disrupting the cells by centrifugation at 15 000 rpm at 4 °C for 10 min. After discarding the supernatant, the pellets were resuspended in 1 mL 4 °C methanol and incubated in the dark for a minimum of 2 h. One last centrifugation was conducted at 15 000rpm and 4 °C, and the green supernatant was separated from the blue pellet to measure its absorbance at 665 and 720 nm against a methanol blank. The chlorophyll$_a$ content was calculated using the formula: $Chl_a(\mu g\ mL^{-1}) = 12.9447(A_{665nm} - A_{720nm})$.[44]

Adherence Test based on Crystal Violet Staining: The procedure was adapted from Wey et al.[14] Briefly, the graphite-foil-based electrodes were cut to yield 1-cm diameter disks and placed at the bottom of a glass-bottom 24-well plate (MatTek Life Sciences). Cells harvested in their mid-to-late exponential state were pelleted in 1.5 mL Eppendorf tubes at 5000 rpm, 25 °C for 10 min, washed with 1xBG11, and concentrated to achieve an optical density OD_{750} = 10 in 1xBG11. 100µL aliquots of the cell suspensions (or of 1xBG11 medium for negative controls) were deposited onto the electrodes and incubated for 16 h in the dark at 30 °C. Following incubation, 80 µL of the supernatant was removed and samples were washed once with 100µL 1xBG11 medium. The remaining cells were stained by adding 100 µL of a 0.01 wt.% crystal violet aqueous solution (Sigma Aldrich) onto the electrodes and incubating at room temperature for 15 min. The stain was removed and samples were washed twice with 100 µL deionized water until no purple color was clearly visible in the washing liquid. 1mL DMSO (Sigma Aldrich) was added to the wells and the plate was shaken at 600 rpm and room temperature for 15 min. The absorbance of crystal violet at 600 nm in the samples was finally measured against a DMSO blank.

Zeta Potential: Cells were grown to their mid-to-late exponential stage, and 2 mL for each sample was harvested in 2 mL Eppendorf tubes. Samples were pelleted, and the supernatants were removed by centrifugation at 5000 rpm for 10 min at room temperature. The pellets were then washed with 1 mL 1 mM HEPES buffer (pH 7.4) and diluted in the same buffer to reach an optical density OD_{750} = 1 in 1 mL. Samples were inserted in DTS1070 electrocapillary cells (Malvern) and the zeta potential measurements were conducted with the Zetasizer NanoZS (Malvern).

Electrochemical Characterization: Measurements were taken by inserting the graphite-based (bio)anodes in a three-electrode system as the working electrode alongside a Pt counter electrode (wire or plate) and an Ag/AgCl reference electrode. The system was connected to a Multi-Palmsens4 potentiostat (Palmsens BV) equipped with the Multitrace 4.4 software. PBS was used as the electrolyte in unmediated conditions and supplemented with 1 mM $K_3Fe(CN)_6$ (Sigma Aldrich) in mediated conditions. Light exposure was provided by a white LED lamp of intensity 370 µE.

Chronoamperometry Experiments under Unmediated Conditions: Multi-step chronoamperometry experiments were conducted in a sequence of 4-h long steps at the increasing applied potentials 100, 200, 300, and 400 mV (vs Ag/AgCl). For each cycle, the system was exposed to 2 h of darkness followed by 1 h of light and a final 30 min of darkness.

Chronoamperometry experiments were conducted over 15 h at a constant applied potential of 300 mV (vs Ag/AgCl). The system was left to equilibrate for 3 h in the dark before being exposed to eight 1-h light–30-min dark cycles. For experiments involving (3-(3,4-dichlorophenyl)-1,1-dimethylurea) (DCMU, Sigma Aldrich), samples were incubated for 15 min in a 50 µM solution of DCMU diluted in PBS from a 10 mM stock in DMSO. Chronoamperometry measurements were taken after incubation.

Cyclic Voltammetry Experiments under Mediated Conditions: The EASA of bare graphite and PPy-coated electrodes were measured under mediated conditions and daylight. The initial applied potential started at 0.0V and was cycled in the positive direction before cycling in the negative direction over the range of [−0.2V; 0.5V] with a 1-mV step for 3 cycles (i.e., until system stabilization). Scan rates started at 15 mV s^{-1} and were decreased to 10, 7.5, 5, 2, and 1 mV s^{-1}. In this potential range, the anodic current peak of the $K_3Fe(CN)_6$ was well-defined and the value was extracted from the 3rd cycle at each scan rate using the PSTrace 5.9 software. A linear fit (with a forced 0 intercept) of the anodic current peak value plotted against the square root of the scan rate was obtained using the Origin 2021b software. The calculated slope was used in the Randles–Sevcik equation[45] using a diffusion coefficient of $D(K_3Fe(CN)_6) = 7.2\times10^{-10}$ m^2 s^{-1}.[46] The photoresponse was conducted at an applied potential starting at 0.0 V that was then cycled in the positive direction before cycling in the negative direction over the range of [−0.2V; 0.5V] with a 1-mV step for 3 cycles (i.e., until system stabilization). A scan rate of 5 mV s^{-1} was used, and the system was left to incubate for 30 min in the dark or light before measurement.

Electrochemical Impedance Spectroscopy Experiments: The EIS response of abiotic electrodes was recorded at V_{DC} = 220 mV and V_{AC} = 5mV in phosphate buffer supplemented with 10 mM $K_3Fe(CN)_6$ in the frequency range of 100 mHz to 1 kHz. To stabilize the surface interface, the open circuit potential of the system and cyclic voltammograms were recorded in the same solution prior to collecting EIS spectra.

Morphological Characterization Abiotic Electrodes: SEM and EDX measurements were conducted using a Zeiss Merlin microscope with an Oxford Instrument X-max Extreme EDX detector and Aztec software (Oxford Instruments). Confocal Raman spectroscopy measurements were performed using an inVia Raman Microscope (Renishaw). Spectra were recorded at an excitation wavelength of 532 nm (1% laser power) in the 600–2000 cm^{-1} range using a 100x objective and a diffraction grating of 1800 cm^{-1}.

Imaging of Biotic Electrodes: The samples were prepared as described for the crystal violet staining just before the dye incubation step. For the optical imaging, the samples were air dried for 30 min before being fastened between 2 glass slides. (Figure S11A, Supporting Information) The cells were imaged in widefield mode using a custom-built optical setup consisting of an inverted microscope (Eclipse Ti-U, Nikon AG Instruments) with an oil-immersion TIRF 100 x objective (N.A. 1.49, Nikon) and an EMCCD camera (iXon Ultra 888, Andor) coupled to a spectrometer (Shamrock 303i, Andor) operated in mirror mode (flat mirror, Al+MgF_2 protected). Samples were illuminated using a TriLine LaserBank system (Cairn Research) at 640 nm, and the cell autofluorescence was detected using a CY5 filter (Chroma). Images were acquired using the Nikon NIS-Elements software (Nikon Instruments) and treated with the Fiji (ImageJ) software.

For the SEM imaging, cells were fixed with 2% paraformaldehyde and 0.2% glutaraldehyde in 0.1 M cacodylate buffer (pH 7.2) for 3 h, washed with 0.1 M cacodylate buffer (pH 7.2), and dehydrated with dimethylformamide (DMF) at increasing concentrations (25%, 50%, 75%, and 90%).

Samples were stored at −20 °C before imaging using a Zeiss Merlin microscope with an Oxford Instrument X-max Extreme EDX detector and Aztec software (Oxford Instruments).

Four-Point Probe Experiment: Graphite foil-based electrodes were prepared as described above. The sheet resistance of both uncoated and PPy-coated samples was measured using an Ossila four-point probe system with Ossila Sheet Resistance v2.0.3.3 software.

Supporting Information

Supporting Information is available from the Wiley Online Library or from the author.

Acknowledgements

The authors acknowledge Dr. Lucie Navratilova from the interdisciplinary center for electron microscopy (CIME) and Hanxuan Wang (LNB) for the SEM characterization. The authors are thankful for support from the Swiss National Science Foundation (Project number CRSII5_205925 and IZLIZ2_182972).

Open access funding provided by Ecole Polytechnique Federale de Lausanne.

Conflict of Interest

The authors declare no conflict of interest.

Data Availability Statement

The data that support the findings of this study are available from the corresponding author upon reasonable request.

Keywords

biophotovoltaics, electrogenicity, polypyrrole, synechocystis sp. PCC6803, synechococcus elongatus PCC7942

Received: October 31, 2022
Revised: February 16, 2023
Published online:

[1] C. Howe, P. Bombelli, *Joule* **2020**, *4*, 2065.
[2] M. Sawa, A. Fantuzzi, P. Bombelli, C. Howe, K. Hellgardt, P. Nixon, *Nat. Commun.* **2017**, *8*, 1327.
[3] K. Rabaey, W. Verstraete, *Trends Biotechnol.* **2005**, *23*, 291.
[4] B. Logan, B. Hamelers, R. Rozendal, U. Schröder, J. Keller, S. Freguia, P. Aelterman, W. Verstraete, K. Rabaey, *Environ. Sci. Technol.* **2006**, *40*, 5181.
[5] L. Wey, P. Bombelli, X. Chen, J. Lawrence, C. Rabideau, S. Rowden, J. Zhang, C. Howe, *ChemElectroChem* **2019**, *6*, 5375.
[6] J. Tschörtner, B. Lai, J. Krömer, *Front. Microbiol.* **2019**, *10*, 866.
[7] D. Lea-Smith, P. Bombelli, R. Vasudevan, C. Howe, *Biochim. Biophys. Acta, Bioenerg.* **2016**, *1857*, 247.
[8] T. Tanaka, N. Kashiwagi, T. Ogawa, *J. Chem. Technol. Biotechnol.* **1988**, *42*, 235.
[9] J. Pisciotta, Y. Zou, I. Baskakov, *PLoS One* **2010**, *5*, e10821.
[10] J. Pisciotta, Y. Zou, I. Baskakov, *Appl. Microbiol. Biotechnol.* **2011**, *91*, 377.
[11] G. Saper, D. Kallmann, F. Conzuelo, F. Zhao, T. Tóth, V. Liveanu, S. Meir, J. Szymanski, A. Aharoni, W. Schuhmann, A. Rothschild, G. Schuster, N. Adir, *Nat. Commun.* **2018**, *9*, 2168.
[12] L. Wey, J. Lawrence, X. Chen, R. Clark, D. Lea-Smith, J. Zhang, C. Howe, *Electrochim. Acta* **2021**, *395*, 139214.
[13] A. Antonucci, M. Reggente, C. Roullier, A. J. Gillen, N. Schuergers, V. Zubkovs, b. P. Lambert, M. Mouhib, E. Carata, L. Dini, A. A. Boghossian, *Nat. Nanotechnol.* **2022**, *17*, 1111.
[14] N. Sekar, R. Jain, Y. Yan, R. Ramasamy, *Biotechnol. Bioeng.* **2015**, *113*, 675.
[15] E. Clifford, R. Bradley, L. Wey, J. Lawrence, X. Chen, C. Howe, J. Zhang, *Chem. Sci.* **2021**, *12*, 3328.
[16] H. Meng, W. Zhang, H. Zhu, F. Yang, Y. Zhang, J. Zhou, Y. Li, *Biotechnol. Biofuels* **2021**, *14*, 109.
[17] M. Mouhib, A. Antonucci, M. Reggente, A. Amirjani, A. Gillen, A. Boghossian, *Nano Res.* **2019**, *12*, 2184.
[18] L. Liu, S. Choi, *J. Power Sources* **2021**, *506*, 230251.
[19] T. Wenzel, D. Härtter, P. Bombelli, C. Howe, U. Steiner, *Nat. Commun.* **2018**, *9*, 1299.
[20] X. Chen, J. M. Lawrence, L. T. Wey, L. Schertel, Q. Jing, S. Vignolini, C. J. Howe, S. Kar-Narayan, J. Z. Zhang, *Nat. Mater.* **2022**, *21*, 811.
[21] M. Reggente, S. Politi, A. Antonucci, E. Tamburri, A. A. Boghossian, *Adv. Mater. Technol.* **2020**, *5*, 1900931.
[22] T. Zajdel, M. Baruch, G. Méhes, E. Stavrinidou, M. Berggren, M. Maharbiz, D. Simon, C. Ajo-Franklin, *Sci. Rep.* **2018**, *8*, 15293.
[23] R. Song, Y. Wu, Z. Lin, J. Xie, C. Tan, J. Loo, B. Cao, J. Zhang, J. Zhu, Q. Zhang, *Angew. Chem.* **2017**, *129*, 10652.
[24] D. Wang, J. Pan, M. Xu, B. Liu, J. Hu, S. Hu, S. Liang, *J. Power Sources* **2021**, *483*, 229220.
[25] A. Kisieliute, A. Popov, R. Apetrei, G. Cârâc, I. Morkvenaite-Vilkonciene, A. Ramanaviciene, A. Ramanavicius, *Chem. Eng. J.* **2019**, *356*, 1014.
[26] Y. Yu, H. Chen, Y. Yong, D. Kim, H. Song, *Chem. Commun.* **2011**, *47*, 12825.
[27] Y. Zou, J. Pisciotta, I. Baskakov, *Bioelectrochemistry* **2010**, *79*, 50.
[28] G. Buscemi, D. Vona, P. Stufano, R. Labarile, P. Cosma, A. Agostiano, M. Trotta, G. Farinola, M. Grattieri, *ACS Appl. Mater. Interfaces* **2022**, *14*, 26631.
[29] Y. Zou, J. Pisciotta, R. B. Billmyre, I. V. Baskakov, *Biotechnol. Bioeng.* **2009**, *104*, 939.
[30] S. Politi, R. Carcione, E. Tamburri, R. Matassa, T. Lavecchia, M. Angjellari, M. Terranova, *Sci. Rep.* **2018**, *8*, 17045.
[31] C. Zhong, Z. Tian, Z. Tian, *J. Phys. Chem.* **1990**, *94*, 2171.
[32] T. Vernitskaya, O. Efimov, *Russ. Chem. Rev.* **1997**, *66*, 443.
[33] K. Keothongkham, S. Pimanpang, W. Maiaugree, S. Saekow, W. Jarernboon, V. Amornkitbamrung, *Int. J. Photoenergy* **2012**, *2012*, 671326.
[34] A. Ramanavicius, A. Finkelsteinas, H. Cesiulis, A. Ramanaviciene, *Bioelectrochemistry* **2010**, *79*, 11
[35] M. Martini, T. Matencio, N. Alonso-Vante, M. A. De Paoli, *J. Braz. Chem. Soc.* **2000**, *11*, 50.
[36] W. Schmidt, G. Drews, J. Weckesser, I. Fromme, D. Borowiak, *Arch. Microbiol.* **1980**, *127*, 209.
[37] E. Hoiczyk, A. Hansel, *J. Bacteriol.* **2000**, *182*, 1191.
[38] A. Antonucci, M. Reggente, A. J. Gillen, C. Roullier, B. P. Lambert, A. A. Boghossian, *Photochem. Photobiol. Sci.* **2022**, *22*, 103.
[39] E. Nagar, S. Zilberman, E. Sendersky, R. Simkovsky, E. Shimoni, D. Gershtein, M. Herzberg, S. S. Golden, R. Schwarz, *Environ. Microbiol.* **2017**, *19*, 2862.
[40] D. Bhaya, N. Bianco, D. Bryant, A. Grossman, *Mol. Microbiol.* **2000**, *37*, 941.
[41] S. Yoshihara, X. Geng, S. Okamoto, K. Yura, T. Murata, M. Go, M. Ohmori, M. Ikeuchi, *Plant and Cell Physiol.* **2001**, *42*, 63.

[42] R. Parnasa, E. Nagar, E. Sendersky, Z. Reich, R. Simkovsky, S. Golden, R. Schwarz, *Sci. Rep.* **2016**, *6*, 32209.
[43] R. Rippka, R. Stanier, J. Deruelles, M. Herdman, J. Waterbury, *Microbiology* **1979**, *111*, 1.
[44] R. Ritchie, *Photosynth. Res.* **2006**, *89*, 27.
[45] N. Elgrishi, K. Rountree, B. McCarthy, E. Rountree, T. Eisenhart, J. Dempsey, *J. Chem. Educ.* **2018**, *95*, 197.
[46] J. Moldenhauer, M. Meier, D. Paul, *J. Electrochem. Soc.* **2016**, *163*, H672.